Published in final edited form as:
Nat Chem Biol. 2014 July ; 10(7): 582–589. doi:10.1038/nchembio.1545.

PIP_2 regulates psychostimulant behaviors through its interaction with a membrane protein

Peter J. Hamilton[#1,9], **Andrea N. Belovich**[#2], **George Khelashvili**[3], **Christine Saunders**[2], **Kevin Erreger**[4,9], **Jonathan A. Javitch**[5,6], **Harald H. Sitte**[7], **Harel Weinstein**[3,8], **Heinrich J.G. Matthies**[4,9,*], and **Aurelio Galli**[1,2,4,9,*]

[1]Vanderbilt Brain Institute, Vanderbilt University School of Medicine, Nashville, TN 37232-8548, United States

[2]Department of Pharmacology, Vanderbilt University School of Medicine, Nashville, TN 37232-8548, United States

[3]Department of Physiology and Biophysics, Weill Cornell Medical College of Cornell University, New York, New York 10065, United States

[4]Department of Molecular Physiology & Biophysics, Vanderbilt University School of Medicine, Nashville, TN 37232-8548, United States

[5]Department of Psychiatry, Columbia University College of Physicians & Surgeons, New York, New York 10032, United States

[6]Department of Pharmacology, Columbia University College of Physicians & Surgeons, New York, New York 10032, United States

[7]Institute of Pharmacology, Center for Physiology and Pharmacology, Medical University Vienna, Vienna, Austria

[8]HRH Prince Alwaleed Bin Talal Bin Abdulaziz Alsaud Institute of Computational Biomedicine, Weill Cornell Medical College of Cornell University, New York, New York 10065, United States

[9]Neuroscience Program in Substance Abuse, Vanderbilt University School of Medicine, Nashville, TN 37232-8548, United States

[#] These authors contributed equally to this work.

Abstract

Correspondence should be addressed to either of the following: Aurelio Galli, Room 7124, MRB III, or Heinrich J. G. Matthies, Room 7141A, MRB III, aurelio.galli@vanderbilt.edu, heinrich.j.matthies@vanderbilt.edu, Vanderbilt University School of Medicine, 465 21st Avenue South, Nashville, TN 37232-8548, USA.

Contributions P.J.H., A.N.B, G.K., C.S., K.E., and H.J.G.M performed experiments. P.J.H., A.N.B, G.K., C.S., K.E., J.A.J., H.H.S, H.W., H.J.G.M, and A.G. designed experiments and analyzed data. G.K. and H.W. generated computational models and analyses. J.A.J. supplied expression vectors and plasmid DNA. P.J.H., A.N.B, H.W., H.J.G.M, G.K, and A.G. wrote the manuscript. All authors participated in the discussion of results and contributed to the preparation of the manuscript.

[*] These authors contributed equally to this work.

Competing interests: The authors declare no competing financial interests.

Europe PMC Funders Author Manuscripts

Phosphatidylinositol (4,5)-bisphosphate (PIP_2) regulates the function of ion channels and transporters. Here, we demonstrate that PIP_2 directly binds the human dopamine (DA) transporter (hDAT), a key regulator of DA homeostasis and a target of the psychostimulant amphetamine (AMPH). This binding occurs through electrostatic interactions with positively charged hDAT N-terminal residues and is shown to facilitate AMPH-induced, DAT-mediated DA efflux and the psychomotor properties of AMPH. Substitution of these residues with uncharged amino acids reduces hDAT-PIP_2 interactions and AMPH-induced DA efflux, without altering the hDAT physiological function of DA uptake. We evaluated, for the first time, the significance of this interaction *in vivo* using locomotion as a behavioral assay in *Drosophila melanogaster*. Expression of mutated hDAT with reduced PIP_2 interaction in *Drosophila* DA neurons impairs AMPH-induced locomotion without altering basal locomotion. We present the first demonstration of how PIP_2 interactions with a membrane protein can regulate the behaviors of complex organisms.

Keywords

dopamine; transporter; amphetamine; *Drosophila melanogaster*; phosphatidylinositol 4,5-bisphosphate

INTRODUCTION

The functional regulation of plasma membrane proteins by lipid molecules is an integral component of cell function and metabolism[1,2]. Phosphatidylinositol (4,5)-bisphosphate (PIP_2) is the phospholipid precursor of the second messengers inositol trisphosphate (IP_3), diacylglycerol (DAG), and phosphatidylinositol (3,4,5)-trisphosphate (PIP_3), and is, itself, capable of acting as a second messenger and cofactor for regulating protein function[1,3-6]. Additionally, PIP_2 has been shown to modulate, through electrostatic interactions, the *in vitro* function of ion channels and transporters, including the serotonin transporter (SERT)[1,7]. A sizeable research effort has been dedicated to determining the diversity of cellular roles for PIP_2 and defining the ubiquity of its electrostatic interactions with various plasma membrane proteins, but how these interactions might modulate the behaviors of complex organisms *in vivo* has never been studied.

The plasma membrane dopamine (DA) transporter (DAT) is a presynaptic protein that plays a pivotal role in regulating DA neurotransmission by mediating the high-affinity reuptake of synaptically-released DA. Gene knockout experiments in multiple organisms, including *Drosophila melanogaster*[8,9], point to the DAT as the main target for the locomotor stimulatory effects of amphetamine (AMPH)[10]. AMPH's addictive properties are mediated, at least in part, through elevation of extracellular DA by inducing DA efflux through the DAT[11,12]. Thus, in order to target and limit AMPH actions pharmacologically, it is essential to understand how to precisely manipulate the DAT to prevent DA efflux without altering its physiological function of DA uptake.

The DAT N-terminus is a structural domain of functional significance. AMPH targets the N-terminus to cause posttranslational modifications (e.g. phosphorylation[13]), which are essential for AMPH to cause DA efflux[14,15] and behaviors[8]. Notably, DAT localization to plasma membrane lipid rafts is also vital for DA efflux[16] and AMPH-induced behaviors[8]. In

this study, we elucidate how plasma membrane PIP_2, which is enriched in lipid rafts[17,18], dictates specific aspects of the transport cycle through its interactions with the N-terminus of the DAT. In terms of AMPH-induced DA efflux, our experimental and computational data demonstrate that the regulatory effect of PIP_2 stems from its electrostatic association with the N-terminus. Here, we introduce the first animal model (*Drosophila melanogaster*) in which we evaluate the behavioral consequences of altered PIP_2 interactions with a plasma membrane protein. We reveal that DAT-PIP_2 interactions are required for AMPH-induced behaviors, thereby presenting PIP_2 and its synthetic pathway as novel regulators of AMPH abuse.

RESULTS

DAT associates with PIP_2

In this study, we aimed to determine the modalities of the regulatory function of PIP_2 in terms of DA homeostasis and AMPH actions. We hypothesized that this regulatory function may be mediated through a physical association between DAT and PIP_2. Using live confocal imaging, we show that in hDAT cells, GFP-hDAT (green) co-localized (yellow) with a plasma membrane PIP_2 sensor (red) (Fig. 1a). As a PIP_2 sensor, we used the pleckstrin homology (PH) domain from phospholipase C_δ ($PHPLC_\delta$-mRFP) that binds specifically to PIP_2 at the plasma membrane and has been used to monitor pools of PIP_2[19]. In these cells, we further probed the association of hDAT with PIP_2 by immunoprecipitating (IP) PIP_2 with an anti-PIP_2 antibody and immunoblotting the immunoprecipitates for DAT (IB) with an anti-DAT antibody (see below). These data strongly suggest that PIP_2 associates with hDAT in this cell line. To reveal the association between PIP_2 and DAT in brain tissue, immunoprecipitations were performed from the striatal tissue of wild-type mice (WT; in presence (+) or absence (−) of the anti-PIP_2 antibody) or DAT knock out (KO) mice[10] (Fig. 1b). In contrast to WT mice, DAT-PIP_2 association was lacking in DAT KO mice. Moreover, in the absence (−) of the PIP_2 antibody, no immunoreactivity was detected. These data demonstrate that PIP_2 associates with the DAT both in cell culture and *ex vivo*.

The DAT N-terminus interacts directly with PIP_2

PIP_2 is negatively charged at physiological pH[20]. Electrostatic interactions between PIP_2 and target proteins are thought to lead to changes in protein conformation and, subsequently, their activity[1,21]. It is recognized that PIP_2 binds positively charged (basic) residues, such as Arg and Lys, possibly in proximity to one or more hydrophobic amino acids[1]. Recently, residues K352 and K460 of the SERT (a DAT homolog) have been identified *in vitro* as possible sites that mediate SERT-PIP_2 association[7]. In the DAT, the homologous amino acids to K352 and K460 are Lys at position 337 (K337) and Arg at position 443 (R443). We reasoned that these two DAT residues represent possible PIP_2 binding sites of functional significance. However, charge-neutralizing substitution of K337 and R443 to Ala (hDAT K337A-R443A), to prevent the interaction of these residues with PIP_2, caused substantial trafficking of the DAT away from the plasma membrane, as assessed by cell surface biotinylation. The amount of hDAT K337A-R443A at the cell surface was reduced by 82.6 ± 5.2% ($p \leq 0.01$ by Student's t-test; $n = 7$) with respect to hDAT. Therefore, in DAT, in contrast to SERT, these two residues support DAT surface expression, preventing us from

determining whether their possible interaction with PIP_2 regulates any mechanistic aspect of the transport cycle.

The N-terminus of the DAT is a structural domain that has been shown to regulate specific aspects of DAT transport cycle, without altering DAT surface expression[14,15,22]. It also contains several Lys and Arg residues (Supplementary Results, Supplementary Fig. 1). We therefore sought to determine whether the N-terminus of the DAT directly interacts with PIP_2 *in vitro*. To this end, we generated a purified recombinant GST-fused N-terminal DAT fragment comprising the first 64 N-terminal amino acids of hDAT (GST-64 hDAT)[23]. The lipid binding analysis of the GST-fusion proteins was conducted using liposomes composed of mixed lipids (phosphatidylcholine, either with or without PIP_2) as previously described[24]. The GST fusion proteins bound to liposomes were pelleted (liposome-pull down) and the binding was assessed by immunoblotting (anti-GST antibody). Figure 2a (top) shows the pull down of GST fusion proteins (GST and GST-64 hDAT) by liposomes containing (+) PIP_2, as compared to liposomes lacking (−) PIP_2. The presence (+) or absence (−) of PIP_2 did not alter pull down of GST alone (GST control). As an additional control, we "sequestered" PIP_2 by preincubating the liposomes with a basic peptide consisting of the sequence of the putative PIP_2 binding domain of the Kv7.2 channel fused to the fatty acid moiety, palmitic acid[25] (pal-HRQKHFEKRR; positively charged at physiological pH)[25]. This peptide is known to interact electrostatically with the polar head groups of PIP_2 to hinder its interaction with plasma membrane proteins[25]. Preincubation of PIP_2-containing liposomes with 3 μM of the basic peptide (pal-HRQKHFEKRR) inhibited pull down of GST-64 hDAT. Figure 2a (bottom) shows quantitation of immunoblots obtained from multiple experiments. Comassie stain was utilized to verify equal loading. These *in vitro* data provide the first evidence of a direct interaction between PIP_2 and a specific region of a neurotransmitter transporter, the DAT N-terminus.

Computational modeling of hDAT interaction with PIP_2

To obtain molecular level structural insights into hDAT N-terminal interactions with PIP_2-containing membranes, we generated a structural context using a previously described homology model of the hDAT[26-28]. To this we have added a recently constructed model of the DAT N-terminus obtained with a combination of structure-prediction methods (Rosetta, Modeller) and atomistic molecular dynamics (MD) simulations (see Methods). These *in silico* modeling steps enabled the prediction of 3-dimensional folds of the N-terminal loop segment composed of hDAT residues 1-59, in the context of the complete transmembrane domain. The resulting hDAT model was used in mean-field-level calculations (SCMFM; see Methods) to quantify the electrostatic interaction of the N-terminus with PIP_2-enriched lipid membranes.

The dominant role of the electrostatic component of the interaction energy between the hDAT N-terminus and PIP_2-containing membranes was substantiated by the shape and the values of the electrostatic potential isosurfaces (EPIs) surrounding the molecular model of the hDAT N-terminal segment shown in figure 2b. The belt-like arrangement of the Lys/Arg residues generates a region of strong positive electrostatic potential (in blue) that favors strong interaction with the negatively charged PIP_2 lipids. Energy-guided docking of this

face of the N-terminus to the membrane model and solving for the steady state distributions of the charged lipid species (PIP_2) under the influence of the electrostatic forces it generates[29-31] produces a quantitative estimate of the electrostatic component of the interaction energy. Thus, the rearrangement of the PIP_2 lipids in the electrostatic field of the N-terminal segment is predicted to result in a significantly increased concentration of PIP_2 near the Lys/Arg belt (Fig. 2c, color coding on the membrane shows the segregation of PIP_2 (blue) to be 2.5 times larger than the PIP_2 ambient concentration (yellow/green)). Particularly notable is the strength of the PIP_2 interaction mediated by DAT residues Lys3 and Lys5. Together, these *in silico* studies suggest that the interactions between the hDAT N-terminus and PIP_2 lipids are driven by electrostatic forces.

Disrupting DAT-PIP_2 interaction inhibits reverse transport

We hypothesized that the functional consequence of DAT-PIP_2 interaction is to support reverse transport of DA. Thus, we disrupted DAT-PIP_2 associations in hDAT cells while recording AMPH-induced DA efflux with amperometry. The amperometric electrode, a carbon fiber electrode juxtaposed to the cell membrane, measures DA efflux by oxidation/reduction reactions, with DA efflux represented as a positive current. To simultaneously record DA efflux while delivering compounds to the intracellular milieu, we combined amperometry with the whole cell patch clamp (APC) technique[9,14]. The whole cell patch electrode controls the intracellular ionic composition, which includes DA[14] (see Methods).

First, we perfused hDAT cells through the whole cell electrode with DA and the basic peptide pal-HRQKHFEKRR (positively charged at physiological pH and tethered to the plasma membrane through the fatty acid moiety, palmitic acid[25]) while recording DA efflux with the amperometric electrode (Fig. 3a). We used this peptide to compete against the DAT N-terminus for PIP_2 interactions as determined in Fig. 2a. Pal-HRQKHFEKRR (3 μM, 10 minutes of intracellular perfusion) was effective in reducing AMPH-induced DA efflux with respect to the efflux obtained with the control peptide pal-HAQKHFEAAA, in which four positive residues were substituted with Ala (Fig. 3a, top). Quantitation of the peak amperometric currents demonstrates that intracellular perfusion of pal-HRQKHFEKRR significantly reduced DA efflux (Fig. 3a, bottom). These data underscore the importance of DAT-PIP_2 interactions in the regulation of DA efflux and point to the type of interactions as electrostatic in nature. We next assessed whether DAT-PIP_2 association regulates other DAT functions (e.g. DAT-mediated inward currents). We recorded hDAT-mediated inward currents from hDAT cells voltage clamped at −60 mV with a whole-cell electrode containing either pal-HRQKHFEKRR or the control peptide pal-HAQKHFEAAA (3 μM, 10 minutes of intracellular perfusion). We stimulated the hDAT-mediated currents by perfusion of either 10 μM AMPH or DA, respectively. In contrast to DA efflux, pal-HRQKHFEKRR failed to inhibit hDAT-mediated inward currents, with respect to the control peptide, either for AMPH (109 ± 4.9% of control; $p \geq 0.8$ by Student's t-test; $n = 4$) or for DA (98 ± 16% of control; $p \geq 0.9$ by Student's t-test; $n = 4$).

To further investigate the role of DAT-PIP_2 interactions in AMPH regulation of DAT function, we transfected hDAT cells with the human muscarinic acetylcholine (ACh) receptor M1 (hM1R), a Gαq coupled receptor. Activation of hM1R activates phospholipase

Europe PMC Funders Author Manuscripts

C (PLC), stimulating hydrolysis of PIP_2 and effectively depleting PIP_2 stores[3]. Live imaging was adopted utilizing mRFP tagged PLC-δ1 PH domain (see Fig. 1a) to detect changes of PIP_2 levels at the plasma membrane induced by ACh, a potent hM1R agonist[32]. In hDAT cells, 5 minutes of ACh (100 μM) decreased surface RFP tagged PLC-δ1 PH domain levels to 64 ± 9% of vehicle control ($p \leq 0.009$ by Student's t-test comparing ACh to vehicle; n = 16). In cells loaded with DA (see Methods), we next quantified the magnitude of AMPH-induced DA efflux before and after bath perfusion of ACh (5 minutes, 100 μM) (Fig. 3b, top). Quantitation of the change in AMPH-induced DA efflux induced by PIP_2 depletion within the same cell (Fig. 3b, bottom) demonstrates that ACh exposure significantly decreased DA efflux. This decrease was not due to a trafficking phenomenon, since exposure of ACh (5 minutes, 100 μM) in hM1R-expressing hDAT cells did not cause significant trafficking of hDAT away from the plasma membrane as compared to vehicle-treated control (Supplementary Fig. 2). We next determined whether providing an excess of intracellular PIP_2 reduces the ability of hM1R agonism to decrease DA efflux. For this, we adopted the APC technique[9,14]. Inclusion of PIP_2 (50 μM) in the whole cell patch pipette solution (10 minutes of intracellular perfusion) impaired the ability of ACh (5 minutes, 100 μM) to significantly decrease AMPH-induced DA efflux with respect to vehicle control (Supplementary Fig. 3). Collectively, these data demonstrate that impairing the electrostatic interaction between PIP_2 and DAT selectively inhibits the ability of AMPH to cause DA efflux.

N-terminal lysine residues mediate DAT-PIP_2 association

Since our *in silico* modeling of the hDAT N-terminus indicated residues Lys3 and Lys5 to be essential in facilitating the electrostatic interaction of PIP_2 with DAT (Fig. 2c), we hypothesized that substitution of these residues with uncharged amino acids (e.g. alanine or asparagine) would disrupt DAT-PIP_2 associations. To probe this inference *in silico*, Lys3 and Lys5 were both substituted computationally with either Ala (hDAT K/A) or with Asn (hDAT K/N), and the resulting constructs (N-terminus of hDAT K/A and hDAT K/N) were evaluated for any conformational rearrangements due to the mutations. The constructs were used in the same computational protocols described for the hDAT model. The results for the mutant constructs show significantly reduced electrostatic interactions with PIP_2-containing membranes for both hDAT K/A (Fig. 4a, compare to Fig. 2c) and hDAT K/N (Supplementary Fig. 4, compare to Fig. 2c).

The inferences from the computational evaluation of the N-terminus association with PIP_2 lipids *in silico* were probed biochemically by determining the effect of charge neutralizing mutations of Lys3 and Lys5. In hDAT K/A cells, we immunoprecipitated PIP_2 and immunoblotted the immunoprecipitates for DAT (IB: anti-DAT). The amount of DAT recovered in the PIP_2 immunoprecipitates was reduced in the hDAT K/A cells compared to the hDAT cells (Fig. 4b, top lane). In the absence of antibody against PIP_2, no signal was detected for DAT in the immunoprecipitates (Fig. 4b, middle lane, IP: beads). The total DAT in the hDAT K/A cells was not decreased with respect to hDAT cells (Fig. 4b, bottom lane; Total DAT). These data demonstrate that substitution of Lys3 and Lys5 decreases DAT-PIP_2 interaction, as predicted from the computational modeling. Quantitation of multiple experiments (n = 4) is shown in figure 4b (bottom). Next, we determined whether

substitution N-terminal Lys3 and Lys5 to Ala impairs the direct interaction of DAT with PIP_2 *in vitro*. We generated a purified recombinant GST-fused N-terminal DAT fragment comprising the first 64 N-terminal amino acids of hDAT with Lys3 and Lys5 substituted to Ala (GST-64 hDAT K/A). The lipid binding analysis of the GST-fusion proteins (either GST-64 hDAT or GST-64 hDAT K/A) was conducted utilizing liposome-pull down as in figure 2. The inset in figure 4b shows the pull down of the GST fusion proteins by liposomes containing PIP_2. Quantitation of immunoblots obtained from multiple experiments demonstrated that pull down of GST-64 hDAT was significantly inhibited by Lys to Ala substitution (GST-64 hDAT K/A was 45 ± 20% of GST-64 hDAT; $p \leq 0.037$ by Student's t-test; n = 4).

In order to assess whether DAT physiological function is altered by disrupting DAT-PIP_2 association, we examined radioactive [^{3}H]DA uptake in both hDAT and hDAT K/A cells. In hDAT K/A cells, the maximal velocity of DA influx (V_{max}) and the apparent DA affinity (K_m) were not significantly different from those of hDAT (Fig. 5a, top). A representative plot of DA uptake kinetics (in triplicate) for hDAT and hDAT K/A is shown in Fig. 5a (bottom), demonstrating that the uptake of substrate is not regulated by the interaction with PIP_2. Consistent with the uptake data, no significant difference was found in the whole-cell DAT-mediated inward current (recorded at −60 mV) between hDAT and hDAT K/A cells upon stimulation with 10 μM DA. The hDAT K/A inward currents were expressed as a percent of hDAT-mediated currents (103 ± 20% of hDAT; $p \geq 0.97$ by Student's t-test; n = 4).

Our pharmacological manipulations (Fig. 3) indicate that disrupting DAT-PIP_2 association has no effect on DAT-mediated DA uptake or DA-induced inward currents but inhibits the ability of AMPH to cause DA efflux. Consistent with this, hDAT K/A cells were found to display strikingly reduced AMPH-induced DA efflux (Fig. 5b, top). Quantitation of the amperometric recordings demonstrate that the Lys to Ala substitution not only decreased DAT-PIP_2 association (Fig. 4), but also decreased the ability of AMPH to cause DA efflux (Fig. 5b, bottom). The reduced AMPH-induced DA efflux was not associated with a reduction in either total or DAT surface expression as assessed by measuring changes in DAT proteins in the total and biotinylated fraction, respectively. Surface fractions were quantitated, normalized to total DAT, and expressed as a percent of hDAT (hDAT K/A was 122 ± 31% of hDAT; $p \geq 0.53$ by Student's t-test; n = 7-8). The findings in the hDAT K/A cells were mirrored by those obtained in the hDAT K/N cells in terms of both DAT-PIP_2 association and hDAT cell surface expression (Supplementary Fig. 5a and 5b). The hDAT K/N also displayed normal uptake (Supplementary Fig. 5c) and, like the hDAT K/A, had a significant reduction in AMPH-induced DA efflux (Supplementary Fig. 5d). Furthermore, AMPH uptake assays revealed that hDAT, hDAT K/A, and hDAT K/N cells displayed comparable AMPH transport (see Methods) (hDAT K/A: 101 ± 4.9% and hDAT K/N: 93.9 ± 17% relative to hDAT; $p \geq 0.88$ by one-way ANOVA; n = 3, in triplicate). These results demonstrate that the reduced ability of AMPH to cause DA efflux promoted by the Lys to Ala substitutions does not involve changes in the surface expression or changes in ability of the DAT mutants to transport AMPH. Another possibility for this decrease in DA efflux is that the N-terminal Lys substitution (hDAT K/A) perturbs the potential AMPH-induced

phosphorylation of the Ser2 and Ser4 adjacent to these Lys residues by altering primary sequence requirements for phosphorylation. To explore this, we substituted Ser2 and Ser4 with Asp (to mimic phosphorylation) in the hDAT K/A background (hDAT K/A-S/D). Cells expressing hDAT K/A-S/D exhibited significantly reduced AMPH-induced DA efflux, similar to hDAT K/A cells (Supplementary Fig. 6a, top). Quantitation of the amperometric recordings demonstrated that Ser to Asp substitution at positions 2 and 4 in the hDAT K/A background did not rescue the ability of AMPH to cause DA efflux (Supplementary Fig. 6a, bottom). The reduced AMPH-induced DA efflux was not associated with a reduction in DA uptake (Supplementary Fig. 6b). These data demonstrate that the reduction in DA efflux caused by substitution of Lys3 and Lys5 with uncharged amino acids cannot be attributed to impaired phosphorylation of adjacent Ser residues.

Reduced DAT-PIP_2 interaction impairs psychomotor behavior

Locomotion is an elemental behavior regulated by DA across species, including *Drosophila melanogaster*[8,9,33,34]. Recently, locomotion in flies has been adopted to evaluate molecular discoveries of AMPH actions mechanistically *in vivo*[8,9]. Thus, *Drosophila* offer a powerful model for elucidating the impact of altered DAT-PIP_2 interactions on locomotion and on the psychomotor stimulant effects of AMPH.

To generate fly lines expressing either hDAT or hDAT K/A selectively in DA neurons, we used the Gal4/UAS system to express a single copy of either hDAT or hDAT K/A in flies with a *Drosophila* DAT (dDAT) null background (dDAT KO; flies are homozygous for the dDAT null allele, DAT^{fmn})[9,35]. Using phiC31-based integration, we generated transgenic flies expressing comparable mRNA levels for hDAT or hDAT K/A. Locomotion of flies was quantified by beam crossing detection over a >24 hour period (data binned in 15 minute intervals) including both the light (horizontal white bar) and the dark (horizontal black bar) cycle. While dDAT KO flies were hyperactive[35], dDAT KO flies expressing hDAT in DA neurons displayed reduced basal locomotion in comparison to dDAT KO (Fig. 6a, compare hDAT to dDAT KO). These data demonstrate the validity of expressing hDAT in *Drosophila* for behavioral studies.

We hypothesized that flies harboring the hDAT K/A would demonstrate comparable locomotion with respect to hDAT expressing flies, since no difference in DA uptake was observed. Figure 6a demonstrates that *Drosophila* expressing hDAT and hDAT K/A displayed comparable basal locomotion, whereas dDAT KO flies exhibited chronically elevated locomotion. Total circadian locomotor activities (24 hour) of hDAT and hDAT K/A flies were not significantly different, while total locomotor activity of dDAT KO flies was significantly higher than hDAT and hDAT K/A (Fig. 6b).

Encouraged by the lack of hyperactivity of hDAT K/A flies under basal conditions, we hypothesized that these flies would have blunted AMPH-induced locomotive behaviors resulting from reduced ability of AMPH to stimulate DA efflux. While AMPH caused a significant increase in locomotion in flies expressing hDAT, this increase was significantly reduced in flies expressing hDAT K/A (Fig. 6c). These data demonstrate, for the first time, the behavioral importance of the interaction of PIP_2 with a plasma membrane protein. This discovery is further enhanced by our ability to associate blunted AMPH-induced behaviors

with a decreased ability of AMPH to cause DA efflux in isolated DA neurons from flies expressing hDAT K/A. *Ex vivo* cultures of *Drosophila* DA neurons were investigated with amperometry to quantify the magnitude of the AMPH-induced DA efflux in the different fly lines. The DA efflux recorded from hDAT K/A expressing neurons was significantly reduced compared to hDAT expressing neurons (Fig. 6d), suggesting that the reduced AMPH-induced locomotion in flies expressing hDAT K/A is due to diminished DA efflux in response to AMPH.

It is possible that this PIP_2 regulation of DA efflux is an evolutionarily conserved mechanism that controls DAT function across phylogeny. To test this possibility, we utilized the APC technique in CHO cells expressing the dDAT (dDAT cells). In dDAT cells, intracellular perfusion of pal-HRQKHFEKRR (3 μM, 10 minutes) was effective in reducing AMPH-induced DA efflux with respect to the efflux obtained with the control peptide pal-HAQKHFEAAA (34.9 ± 12.9% of control peptide; $p \leq 0.01$ by Student's t-test; $n = 3$). These results parallel those obtained in hDAT cells (Fig. 3). In this study, we provide the first behavioral evidence for the relevance of the interaction of PIP_2 with a plasma membrane protein, associating AMPH behaviors to altered neuronal DAT function within the same organism.

DISCUSSION

We recently demonstrated that disrupting the localization of DAT in lipid rafts impairs the ability of AMPH to cause both DA efflux (without altering DA uptake)[16], and associated behaviors[8]. This led us to hypothesize that the molecular underpinnings required for AMPH actions reside in lipid rafts. Raft microdomains are considered scaffolds for PIP_2 signaling, enabling PIP_2 to selectively regulate different cellular processes[36]. Yet, partitioning of PIP_2 into lipid rafts has been criticized as energetically improbable, since PIP_2 consists of a polyunsaturated acyl side chain (arachidonic acid) that is unlikely to spontaneously partition into cholesterol-rich rafts[20]. Therefore, it is theorized that the partitioning of PIP_2 into rafts is facilitated by interactions with raft-localized proteins[20]. Here we demonstrate that PIP_2 directly interacts with hDAT, a protein that localizes to the rafts[16,37,38].

We found that the DAT N-terminus (a domain of functional importance)[14,15] is engaged in direct electrostatic interactions with PIP_2, described by both computational and biochemical analysis. We demonstrate that this interaction is direct and distinct from the recently described association of PIP_2 with SERT[7]. This DAT-PIP_2 interaction, which occurs in brain tissue, involves the two most distal N-terminal Lys (Lys3 and Lys5). These data, combined with the regulatory nature of DAT localization to PIP_2 enriched lipid rafts, led us to hypothesize that PIP_2 participates in coordinating the complex molecular events underlying *specific* DAT activities. This includes AMPH-induced DA efflux. Notably, this interaction does not regulate the physiological function of DAT (DA uptake), DAT surface expression, and AMPH uptake. Other functions of the DAT include AMPH- or DA-stimulated inward currents that represent inward movements of ions associated with the transport of substrate. Therefore, we expected that substrate-induced inward currents would not be affected by disruption of DAT-PIP_2 interaction, in the same way that DA or AMPH uptake is not affected. We show that disrupting DAT-PIP_2 interaction by substitution of

Lys3 and Lys5 with Ala did not impair the ability of hDAT to sustain electrical inward currents stimulated by either DA or AMPH. The regulatory nature of the direct DAT-PIP_2 interaction on DAT-mediated DA efflux is underscored by our results demonstrating that "sequestering" PIP_2, with our palmitoyl-positively charged peptide, or depleting PIP_2, by stimulating PLC activity, results in diminished reverse transport of DA. Consistent with these findings is the notable result that intracellular perfusion of the palmitoyl-positively charged peptide did not impair hDAT-mediated inward currents stimulated by either AMPH or DA relative to control peptide. These data underscore the interaction between DAT and PIP_2 as a key regulator of the specific DAT function of DA efflux.

N-terminal phosphorylation is a requirement for the ability of AMPH to cause a robust DA efflux[14]. The results of our specific molecular manipulations support the notion that Lys to Ala substitution did not impair DA efflux by altering primary sequence requirements for phosphorylation of Ser2 and Ser4. Indeed, pseudophosphorylation of these Ser residues in the hDAT K/A background failed to rescue DA efflux. Consistent with this notion, palmitoyl-positively charged peptide (which does not alter the N-terminus primary sequence) disrupts both the direct interaction of the N-terminus with PIP_2 as well as DA efflux. However, the computational modeling reveals the possibility that the strength of the association of Lys3 and Lys5 with PIP_2 regulates the proper conformation of the DAT N-terminus and affects the transporter N-terminus as a whole. Therefore, we cannot exclude the possibility that the observed DAT-PIP_2 association regulates N-terminal phosphorylation of non-adjacent Ser by coordinating suitable conformations. Nevertheless, this possibility does not diminish the importance of the discovery that DAT-interaction with PIP_2 is a key determinant of AMPH-induced DA efflux and behaviors. On the contrary, it highlights an opportunity, in future studies, to understand whether the DAT N-terminal interaction with PIP_2 supports N-terminal phosphorylation and/or the importance of phosphorylation for N-terminal conformations and DAT-PIP_2 association.

The Ser-Lys-Ser-Lys N-terminal sequence of the DAT is conserved across several species, including *Drosophila*, suggesting that the DAT-PIP_2 association is a possible evolutionarily conserved mechanism that regulates specific DAT functions. Our data demonstrate that disruption of the dDAT-PIP_2 interaction impairs DA efflux, which parallels our results in the hDAT. It is tempting to speculate that this mechanism of N-terminal regulation of transporter function through electrostatic interactions with PIP_2 is a potential mode of regulation for other neurotransmitter transporters as well. Examination of sequences of the N-terminal regions of four major neurotransmitter transporters (hDAT, hSERT, hNET, and hVMAT2) reveals that the positively charged residues are not only abundant in this region, but are also often clustered. In the hDAT, we revealed the consequences of this clustering in a structural context, where one of these clusters contains Lys3 and Lys5, which enables this region to attract PIP_2 lipids. Therefore, a mechanism of PIP_2 regulation, similar to the one outlined here for DAT function, may apply to other neurotransmitter transporters with charged clusters in their N-terminal sequences.

Recently we discovered that the AMPH-induced 5-HT efflux mediated by SERT also relies on PIP_2 interactions with positively-charged residues[7]. However, these residues are not localized to the N-terminus of SERT. These data do not exclude a possible role of SERT N-

terminus basic residues in SERT-PIP_2 interaction and AMPH-induced 5-HT efflux. In contrast, in DAT, mutation (to Ala) of the corresponding SERT-PIP_2 binding sites causes substantial trafficking of DAT away from the plasma membrane, disrupting its membrane expression. Thus, this trafficking phenomenon prevents our ability to determine the significance of these residues in the mechanistic aspects of the DAT transport cycle. However, it is clear that they do not functionally replace Lys3 and Lys5 in terms of DA efflux.

Prior to this work, it was unclear whether the association and/or dissociation of plasma membrane proteins with PIP_2 played a role in the regulation of behaviors of complex organisms. Here, we took advantage of an animal model (*Drosophila melanogaster*) to determine the behavioral consequences of disrupting direct interactions of DAT with PIP_2. *Drosophila* expressing hDAT K/A solely in DA neurons did not display altered circadian locomotor activity. This is not surprising, since the cells expressing hDAT K/A have both normal DA uptake and DA affinity. However, hDAT K/A flies exhibit significant reductions in the behavioral psychomotor responses to AMPH. These data convey the significance of the interaction between PIP_2 and plasma membrane proteins (i.e. DAT) in fundamental organismal behaviors, such as locomotion. The discovery of this PIP_2 regulation of the psychomotor actions of AMPH is further enhanced by our ability to record DA efflux (for the first time) directly from DA neurons cultured from the same *Drosophila* lines utilized in our behavioral assays. DA neurons expressing hDAT K/A have a significant reduction in DA efflux with respect to neurons expressing hDAT. This enhances our molecular discoveries outlining the DAT-PIP_2 interaction as required for DA efflux and obligatory in the ability of AMPH to cause psychomotor behaviors. These data promote PIP_2 and its synthetic pathway from its canonical role as a modulator of cell function and metabolism to a new role as a regulatory agent of both elemental behaviors, such as locomotion, and maladaptive behaviors, such as psychostimulant abuse.

ONLINE METHODS

Cell culture and transfection

The GFP-hDAT-pCIHygro expression vectors containing hDAT, hDAT K/A (Lys3 and Lys5 to Ala), hDAT K/N (Lys3 and Lys5 to Asn), or hDAT K/A-S/D (Lys3 and Lys5 to Ala and Ser2 and Ser4 to Asp) sequence were generated, confirmed and transiently transfected into Chinese hamster ovary (CHO) cells. The *Drosophila* DAT cDNA was generously provided by the laboratory of Dr. Satinder Singh (Yale University). In some experiments (noted in figure legend), stably transfected hDAT CHO cells were used. These cells were generated as previously described[22]. Cells were maintained in a 5% CO_2 incubator at 37°C and maintained in Ham's F-12 medium supplemented with 10% fetal bovine serum (FBS), 1 mM L-glutamine, 100 U/mL penicillin, and 100 μg/mL streptomycin. Stably transfected hDAT CHO cells were kept under selection with 250 μg/mL hygromycin B (Corning Cellgro). Fugene-6 (Roche Molecular Biochemicals) in serum-free media was used to transfect cells using a 6:1 transfection reagent:DNA ratio. Assays were conducted 24-48 hours post transfection.

Drosophila neuron culture

Drosophila neurons were cultured from 1-3 day old males. Brains were dissected in Schneider's medium with 1.5% bovine serum albumen (BSA) and optic lobes were removed. Brains were washed with Schneider's medium and incubated for 40 minutes in collagenase (0.3%) and trypsin (0.125%). They were washed in Schneider's medium supplemented with 10% heat inactivated FBS. Dissociated cells were obtained by brain trituration in medium. Cells from each brain were plated on one poly-D-lysine coated MatTek® dish treated with collagen (type IV). Assays were performed the next day.

Cell imaging

We used the pleckstrin homology (PH) domain from phospholipase C_δ (PHPLC$_\delta$-mRFP) that binds to PIP_2 at the plasma membrane and has been used to monitor pools of PIP_2 at the plasma membrane[19]. Cells on poly-D-lysine coated MatTek® dishes were co-transfected with GFP-DAT and PHPLCδ-mRFP and, after 48 hours, were deprived of serum overnight. Single confocal image sections were generated by using a LSM 510 inverted confocal microscope (Zeiss) by sequential imaging of live cells.

Co-immunoprecipitations

Cells were grown to confluence in 25 cm^2 culture flasks and serum deprived overnight prior to assay. On the day of the assay, cells were washed three times with 4°C phosphate-buffered saline (Gibco) containing 1 mM EGTA and 1 mM EDTA and lysed in RIPA buffer (100 mM NaCl, 1.0% IGEPAL CA-630 (NP-40), 0.5% sodium deoxycholate, 0.1% SDS, 50 mM Tris, pH = 8.0, supplemented with a protease inhibitor cocktail (Sigma Aldrich)). Lysates were passed twice through a 27.5 gauge needle and centrifuged at 15,000 x g for 30 minutes. With a portion of the total cell lysate (TCL) collected to run as the totals, 1 mL of the remaining supernatant was incubated at 4°C for 4 hours with Sepharose-G beads (Fisher Scientific), previously washed with 1% BSA in RIPA buffer and preincubated with 2.5 μg PIP_2 antibody (mouse monoclonal, Enzo Life Sciences). For the negative control, TCL supernatant was incubated with BSA-blocked Sepharose-G beads alone. Beads were spun down, washed with cold RIPA buffer, and samples eluted with Laemmli sample buffer at 95°C for 5 minutes. TCL and eluates were analyzed by SDS-PAGE and immunoblotting (see below for antibody details). Band intensity was quantified using ImageJ software (National Institutes of Health). The association between PIP_2 and hDAT variants was represented as the ratio of eluate:TCL band intensity, normalized to the eluate:TCL ratio observed in hDAT and expressed as a percent. For the mouse DAT-PIP_2 co-immunoprecipitations from striatum, the same protocol was used with the following modifications: striatum was dissected from either wild-type or DAT KO mice, solubilized in RIPA buffer (1:10 weight/volume), homogenized, lysed on ice for 30 minutes and then centrifuged. The remaining protocol was performed as described above. The mice used for these experiments were handled in compliance with IACUC protocols.

Cell surface biotinylation and protein immunoblot

Cells were cultured in 6-well plates. For cell surface biotinylation assays, cells were labeled with sulfo-NHS-SS-biotin (1.0 mg/ml; Pierce) before purification and analysis via SDS-

PAGE/immunoblots[39]. hDAT was detected using a rat monoclonal primary antibody to the N-terminus of hDAT (1:1000) (Millipore Bioscience Research Reagents) and a goat-anti-rat-HRP-conjugated secondary antibody (1:5000; Jackson ImmunoResearch).

Gluthathione transferase (GST) fusion proteins

GST and GST fused to the first 64 N-terminal amino acids of hDAT were purified as described previously[23] with some modifications. Briefly, GST and the GST fusion proteins were produced in *Escherichia coli* BL21 DE3 LysS. The culture was grown at 30°C, expression induced by the addition of 1 mM isopropylβ-d-1-thiogalactopyranoside at 18°C, and the culture was harvested 8 hours after induction. The frozen pelleted bacteria was thawed in Tris-buffered saline (TBS) containing 10% glycerol and a Bacterial Protease inhibitor cocktail (Roche Diagnostics)(pH 7.4) and treated with 1 mg/mL lysozyme followed by 15 mM CHAPS. It was then sonicated and cleared by centrifugation. The lysate was passed over glutathione Sepharose 4B beads (GE Healthcare) and washed several times with TBS, followed by 10 mM Tris containing 10% glycerol and eluted with TBS containing 10 mM gluthathione. The quality, size, and amount (relative to BSA) of GST fusions were determined by SDS-PAGE and Bio-Safe Coomassie G-250 Stain. The amount was determined by analysis of imaged gels using ImageQuantTL.

Liposome binding

GST and GST fusion proteins where incubated with or without liposomes for 10 minutes at room temperature, centrifuged at 100,000 x g for 20 minutes at 4°C, and analyzed by immunoblot analysis using anti-GST antibodies (The Vanderbilt Antibody and Protein Resource Core). Liposomes were formed by extrusion of synthetic lipids at a final concentration of 1 mM. Liposomes were formed in 10 mM HEPES/TRIS, 100 mM NaCl with 95% phosphatidylcholine (DOPC; Echelon) and 5% PIP_2 (Phosphatidylinositol 4,5-bisphosphate diC16) at a pH of 7.4.

Amperometry and patch clamp electrophysiology

Cells were plated at a density of ~20,000 per 35-mm culture dish. To preload cells with DA, dishes were washed with KRH assay buffer (130 mM NaCl, 1.3 mM KCl, 1.2 mM KH_2PO_4, 10 mM HEPES, and 2.2 mM $CaCl_2$, pH 7.4) containing 10 mM dextrose, 100 μM pargyline, 1 mM tropolone, and 100 μM ascorbic acid, and incubated with 1 μM DA in KRH assay buffer for 20 minutes at 37°C. To preload *Drosophila* neurons, dishes were washed with KRH assay buffer (as above) containing 100 nM raclopride, and incubated with 1 μM DA in KRH assay buffer for 20 minutes at 26°C. All dishes were washed three times with the external bath solution (130 mM NaCl, 10 mM HEPES, 34 mM dextrose, 1.5 mM $CaCl_2$, 0.5 mM $MgSO_4$, 1.3 mM KH_2PO_4, adjusted pH to 7.35, and 300 mOsm).

To deliver DA (2 mM, Sigma Aldrich), PIP_2 inhibitory/control peptides (3 μM pal-HRQKHFEKRR or pal-HAQKHFEAAA), and/or PIP_2 (50 μM, phosphatidylinositol 4,5-bisphosphate diC8, Echelon Biosciences), a programmable puller (model P-2000, Sutter Instruments, Novato CA) was used to fabricate quartz recording pipettes with a resistance of 3-5 MΩ. These pipettes were filled with an internal solution containing: 120 mM KCl, 10 mM HEPES, 0.1 mM $CaCl_2$, 2 mM $MgCl_2$, 1.1 mM EGTA, 30 mM dextrose, pH 7.35, and

275 mOsm. Upon gaining access to the cells, the internal solution was allowed to diffuse into the cell for 10 minutes.

Experiments involving perfusion of AMPH or DA (Fig. 3b and inward current experiments) utilized double-barrel quartz tubing with an inner diameter of 250 μm (Polymicro Technologies, Phoneix AZ) placed ~80 μm from the cell. DAT-mediated inward currents were recorded at −60 mV.

To record DA efflux, a carbon fiber electrode (ProCFE; fiber diameter of 5 μm; obtained from Dagan Corporation) juxtaposed to the plasma membrane and held at +700 mV (a potential greater than the oxidation potential of DA) was used to measure DA flux through oxidation reactions. Amperometric currents in response to the addition of AMPH were recorded using an Axopatch 200B amplifier (Molecular Devices, Union City, CA) with a low-pass Bessel filter set at 1 kHz; traces were digitally filtered offline at 1 Hz using Clampex9 software (Molecular Devices, Union City, CA). DA efflux was quantified as the peak value of the amperometric current for all experiments except for recordings from *Drosophila* neurons. For *Drosophila* neurons, total DA efflux was quantified as the integral of the trace for a fixed 15 minute window. Dopaminergic neurons were recognized by fluorescence microscopy since the TH-GAL4 drives the expression of mCherry in dopaminergic neurons.

[^{3}H]DA uptake

Cells were plated on poly-D-lysine coated, 24-well plates and grown to ~90% confluence. On the day of the experiment, cells were washed once with 37°C KRH buffer containing 10 mM dextrose, 100 μM pargyline, 1 mM tropolone, and 100 μM ascorbic acid, and equilibrated for 5 minutes at 37°C. Saturation kinetics of DA uptake was determined using a mixture of [^{3}H]DA (PerkinElmer Life Sciences, Waltham, MA) and unlabeled DA diluting to final DA concentrations of 0.01 μM - 10 μM. Uptake was initiated by bath addition of the dilution row mixture. Uptake was terminated after 10 minutes by washing twice in ice-cold KRH buffer. Scintillation fluid (Optiphase HiSafe 3, PerkinElmer Life Sciences) was added to the wells and the plates were counted in a Wallac Tri-Lux β-scintillation counter (Wallac). Nonspecific binding was determined in the presence of 10 μM cocaine. K_m and V_{max} values were derived by fitting Michaelis-Menten kinetics to the background corrected uptake data, using GraphPad Prism 5.0 (GraphPad Software, San Diego, CA). All determinations were performed in triplicates.

Computational Modeling

To evaluate the interactions between PIP_2-enriched membranes and the N-terminal region of the hDAT (residues 1-59), as well as the hDAT K/A and hDAT K/N mutants, molecular models were constructed with the knowledge-based structure-prediction tool Rosetta[40]. 1,000 different structures obtained from the structure prediction protocols in Rosetta were filtered through clustering according to a criterion of *maximization of common structure conservation* implemented in the in-house algorithm RMSDTT[41], which has been introduced into the molecular graphics program, visual molecular dynamics (VMD)[42]. Clusters with the largest numbers of conformations (usually 2–3 top clusters for each

construct) were selected for further refinement with atomistic molecular dynamics (MD) simulations, to find the motifs within each cluster that were most frequently found in the Rosetta prediction. Predicted structures of the hDAT N-terminus, incorporating these most frequent motifs, were then subjected to both unbiased MD and replica exchange MD[43] simulations to assess the stability of the overall fold of the N-terminus, as well as of the individual structural elements identified with Rosetta.

The top structures that underwent the filtering process, described above, were further examined for suitability in the complete model of the hDAT transmembrane bundle (TMB)[26-28]. The structures were embedded into a compositionally-asymmetric lipid membrane model (5:45:50 mixture of PIP_2/POPE (phosphatidylethanolamine) / POPC (phosphatidylcholine) on the intracellular leaflet, and 30:70 mixture of sphingomyelin / POPC on the extracellular leaflet[44]. Docking of the N-terminus (1-59 residues) to the TMB (residues 57-590) was carried out with Modeller[45]. Specific poses for the N-terminal constructs, relative to the TMB, were selected based on the criterion of positioning the largest positive electrostatic potential isosurfaces (EPIs) towards the membrane surface. As shown before[29], such configurations not only result in the strongest electrostatic interactions between the protein and the PIP_2-containing membrane, but also produce the highest levels of concomitant PIP_2 sequestration by the N-terminal peptide. These juxtamembrane poses of the N-terminus served as starting configurations for subsequent studies of the dynamics of PIP_2 lipids near the hDAT N-terminus, as detailed below.

The protocol used to evaluate the interaction of the hDAT N-terminus with PIP_2-containing membranes is based on the application of the self-consistent mean-field model (SCMFM) that evaluates the steady state distributions of charged lipid species (PIP_2, in this case) under the influence of electrostatic forces from a membrane-adsorbing macromolecule (here, the hDAT N-terminus) and quantifies the corresponding adsorption energies. As described in detail[29-31], the SCMFM is a mesoscale approach, based on the non-linear Poisson-Boltzmann (NLPB) theory of electrostatics[46] and Cahn-Hilliard dynamics[47], in which the protein is considered in 3-dimensional full atomistic detail, and the lipid membrane is considered as a 2-dimensional, tensionless, incompressible low-dielectric elastic slab in which the equilibrium distribution of different lipid species around adsorbing protein is obtained by self-consistent minimization. The governing free energy function contains contributions from electrostatic interactions, lipid mixing entropy, and mixing entropy of mobile salt ions in the solution. The SCMFM calculation of the membrane interaction of the hDAT N-terminus constructs (hDAT and the hDAT K/A or hDAT K/N mutants) considered in full atomistic detail (with partial charge and atomic radii taken from the all-atom CHARMM27 force field with CMAP corrections for proteins[48], was carried out with the N-terminus positioned 2Å away from the lipid surface with average surface charge density of $-0.0031e$ (corresponding to a lipid mixture with 5% PIP_2). The NLPB equation was then solved numerically as described[29-31], in a 0.1 M ionic solution of monovalent counterions (corresponding to λ=9.65Å Debye length), and using a dielectric constant of 2 for membrane interior and protein, and 80 for the solution.

AMPH Uptake

Plated hDAT, hDAT K/N, and hDAT K/A cells, as well as untransfected cells (to account for non-specific AMPH uptake) were washed with KRH assay buffer and incubated for 5 min at 37 °C with 10 nM AMPH. Cells were washed three times with ice-cold KRH and AMPH was extracted with acidic organic solvent. AMPH was quantified by reversed-phase HPLC using the Waters AccQ·Tag® method which uses pre-column derivatized reagents that help separate and easily detect fluorescence adducts (Waters Corporation, Milford, MA). AMPH uptake (with non-specific uptake subtracted) was normalized to hDAT levels and expressed as a percent.

Drosophila Genetics, Molecular Biology, and Construction of UAS hDAT

Flies lacking the *Drosophila* dopamine transporter (DAT^{fmn})[35] and flies harboring TH-Gal4[49] were outcrossed to a control line (Bloomington Indiana (BI) 6326) and selected by PCR or by eye color. TH-GAL4 (Bl 8848) and M{vas-int.Dm}ZH-2A, M{3xP3-RFP.attP′}ZH-22A (Bl 24481) were obtained from the BI stock center and outcrossed to flies lacking the *Drosophila* DAT (DAT^{fmn}) and carrying the *white* (w^{1118}) mutation (BI stock number 6236) for 5–10 generations. Transgenes (hDAT or hDAT K/A) were cloned into pBI-UASC[50], and constructs were injected into embryos from M{vas-int.Dm}ZH-2A, M{3xP3-RFP.attP′}ZH-22A (Bl 24481). Initial potential transformants were isolated by selecting for red eyes and lack of GFP signal in the head. Transformants were also verified by RFP fluorescence and outcrossed 5-8 times to DAT^{fmn} flies. The presence of DAT^{fmn} lesion was verified by PCR. Flies were maintained on a standard cornmeal/molasses/yeast media at 25°C and 65% humidity with a 12 hour/12hour light/dark cycle. Lights came on at 8 AM and off at 8 PM.

Behavioral Analysis

Three-day-old males were collected and placed into tubes with food for three days. After three days locomotion was recorded for 32 hours by beam breaks and analyzed using equipment/software from Trikinetics (www.trikinetics.com). For the AMPH-induced locomotion, males were starved for 6 hours and then fed sucrose (10 mM) containing either AMPH (1 mM) or vehicle.

Statistical Analysis

Compiled data are expressed as normalized mean values ± standard error. For statistical analysis, we used either a Student's t-test or one-way ANOVA depending on the n of the experimental groups. $P < 0.05$ was considered statistically significant.

Supplementary Material

Refer to Web version on PubMed Central for supplementary material.

Acknowledgements

We thank Dr. Satinder Singh (Yale University) for the gift of the *Drosophila* DAT cDNA. Computational resources were provided by Teragrid allocation MCB120008 on the Ranger machine and the David Cofrin Center for Biomedical Information of the Institute for Computational Biomedicine at Weill Cornell Medical College.

Sponsorship: Work supported by NSF Fellowship DGE0909667 and F31 DA 035535-01 (P.J.H.), P22893 (H.H.S.), DA035263 (A.G.), P01 DA12408 (A.G., H.W., J.A.J.), and U54GM087519 (H.W., J.A.J.).

References

1. Suh BC, Hille B. PIP2 is a necessary cofactor for ion channel function: how and why? Annu Rev Biophys. 2008; 37:175–95. [PubMed: 18573078]
2. McLaughlin S, Murray D. Plasma membrane phosphoinositide organization by protein electrostatics. Nature. 2005; 438:605–11. [PubMed: 16319880]
3. Kadamur G, Ross EM. Mammalian phospholipase C. Annu Rev Physiol. 2013; 75:127–54. [PubMed: 23140367]
4. Czech MP. PIP2 and PIP3: complex roles at the cell surface. Cell. 2000; 100:603–6. [PubMed: 10761925]
5. Ben-Aissa K, et al. Activation of Moesin, a Protein That Links Actin Cytoskeleton to the Plasma Membrane, Occurs by Phosphatidylinositol 4,5-bisphosphate (PIP2) Binding Sequentially to Two Sites and Releasing an Autoinhibitory Linker. J Biol Chem. 287:16311–23. [PubMed: 22433855]
6. Whorton MR, MacKinnon R. Crystal structure of the mammalian GIRK2 K+ channel and gating regulation by G proteins, PIP2, and sodium. Cell. 147:199–208. [PubMed: 21962516]
7. Buchmayer F, et al. Amphetamine actions at the serotonin transporter rely on the availability of phosphatidylinositol-4,5-bisphosphate. Proc Natl Acad Sci U S A. 2013; 110:11642–7. [PubMed: 23798435]
8. Pizzo AB, et al. The membrane raft protein Flotillin-1 is essential in dopamine neurons for amphetamine-induced behavior in Drosophila. Mol Psychiatry. 2013; 18:824–33. [PubMed: 22710269]
9. Hamilton PJ, et al. De novo mutation in the dopamine transporter gene associates dopamine dysfunction with autism spectrum disorder. Mol Psychiatry. 2013 [PubMed: 23979605]
10. Giros B, Jaber M, Jones SR, Wightman RM, Caron MG. Hyperlocomotion and indifference to cocaine and amphetamine in mice lacking the dopamine transporter. Nature. 1996; 379:606–12. [PubMed: 8628395]
11. Sulzer D, Sonders MS, Poulsen NW, Galli A. Mechanisms of neurotransmitter release by amphetamines: a review. Prog Neurobiol. 2005; 75:406–33. [PubMed: 15955613]
12. Robertson SD, Matthies HJ, Galli A. A closer look at amphetamine-induced reverse transport and trafficking of the dopamine and norepinephrine transporters. Mol Neurobiol. 2009; 39:73–80. [PubMed: 19199083]
13. Cervinski MA, Foster JD, Vaughan RA. Psychoactive substrates stimulate dopamine transporter phosphorylation and down regulation by cocaine sensitive and protein kinase C dependent mechanisms. J Biol Chem. 2005
14. Khoshbouei H, et al. N-terminal phosphorylation of the dopamine transporter is required for amphetamine-induced efflux. PLoS Biol. 2004; 2:E78. [PubMed: 15024426]
15. Fog JU, et al. Calmodulin kinase II interacts with the dopamine transporter C terminus to regulate amphetamine-induced reverse transport. Neuron. 2006; 51:417–29. [PubMed: 16908408]
16. Cremona ML, et al. Flotillin-1 is essential for PKC-triggered endocytosis and membrane microdomain localization of DAT. Nat Neurosci. 2011; 14:469–77. [PubMed: 21399631]
17. Wang J, Richards DA. Segregation of PIP2 and PIP3 into distinct nanoscale regions within the plasma membrane. Biol Open. 2012; 1:857–62. [PubMed: 23213479]
18. Hope HR, Pike LJ. Phosphoinositides and phosphoinositide-utilizing enzymes in detergent-insoluble lipid domains. Mol Biol Cell. 1996; 7:843–51. [PubMed: 8816992]
19. Varnai P, Balla T. Visualization of phosphoinositides that bind pleckstrin homology domains: calcium- and agonist-induced dynamic changes and relationship to myo-[3H]inositol-labeled phosphoinositide pools. J Cell Biol. 1998; 143:501–10. [PubMed: 9786958]
20. McLaughlin S, Wang J, Gambhir A, Murray D. PIP(2) and proteins: interactions, organization, and information flow. Annu Rev Biophys Biomol Struct. 2002; 31:151–75. [PubMed: 11988466]
21. Hilgemann DW, Ball R. Regulation of cardiac Na+,Ca2+ exchange and KATP potassium channels by PIP2. Science. 1996; 273:956–9. [PubMed: 8688080]

22. Bowton E, et al. Dysregulation of dopamine transporters via dopamine D2 autoreceptors triggers anomalous dopamine efflux associated with attention-deficit hyperactivity disorder. J Neurosci. 2010; 30:6048–57. [PubMed: 20427663]
23. Binda F, et al. Syntaxin 1A interaction with the dopamine transporter promotes amphetamine-induced dopamine efflux. Mol Pharmacol. 2008; 74:1101–8. [PubMed: 18617632]
24. Varnai P, et al. Inositol lipid binding and membrane localization of isolated pleckstrin homology (PH) domains. Studies on the PH domains of phospholipase C delta 1 and p130. J Biol Chem. 2002; 277:27412–22. [PubMed: 12019260]
25. Robbins J, Marsh SJ, Brown DA. Probing the regulation of M (Kv7) potassium channels in intact neurons with membrane-targeted peptides. J Neurosci. 2006; 26:7950–61. [PubMed: 16870740]
26. Beuming T, et al. The binding sites for cocaine and dopamine in the dopamine transporter overlap. Nat Neurosci. 2008; 11:780–9. [PubMed: 18568020]
27. Bisgaard H, et al. The binding sites for benztropines and dopamine in the dopamine transporter overlap. Neuropharmacology. 2011; 60:182–90. [PubMed: 20816875]
28. Kniazeff J, et al. An intracellular interaction network regulates conformational transitions in the dopamine transporter. J Biol Chem. 2008; 283:17691–701. [PubMed: 18426798]
29. Khelashvili G, Galli A, Weinstein H. Phosphatidylinositol 4,5-biphosphate (PIP(2)) lipids regulate the phosphorylation of syntaxin N-terminus by modulating both its position and local structure. Biochemistry. 2012; 51:7685–98. [PubMed: 22950482]
30. Khelashvili G, Harries D, Weinstein H. Modeling membrane deformations and lipid demixing upon protein-membrane interaction: the BAR dimer adsorption. Biophys J. 2009; 97:1626–35. [PubMed: 19751667]
31. Khelashvili G, Weinstein H, Harries D. Protein diffusion on charged membranes: a dynamic mean-field model describes time evolution and lipid reorganization. Biophys J. 2008; 94:2580–97. [PubMed: 18065451]
32. Balla T, Szentpetery Z, Kim YJ. Phosphoinositide signaling: new tools and insights. Physiology (Bethesda). 2009; 24:231–44. [PubMed: 19675354]
33. Wicker-Thomas C, Hamann M. Interaction of dopamine, female pheromones, locomotion and sex behavior in Drosophila melanogaster. J Insect Physiol. 2008; 54:1423–31. [PubMed: 18762189]
34. Pendleton RG, Rasheed A, Sardina T, Tully T, Hillman R. Effects of tyrosine hydroxylase mutants on locomotor activity in Drosophila: a study in functional genomics. Behav Genet. 2002; 32:89–94. [PubMed: 12036114]
35. Kume K, Kume S, Park SK, Hirsh J, Jackson FR. Dopamine is a regulator of arousal in the fruit fly. J Neurosci. 2005; 25:7377–84. [PubMed: 16093388]
36. van Rheenen J, Achame EM, Janssen H, Calafat J, Jalink K. PIP2 signaling in lipid domains: a critical re-evaluation. EMBO J. 2005; 24:1664–73. [PubMed: 15861130]
37. Sorkina T, Caltagarone J, Sorkin A. Flotillins regulate membrane mobility of the dopamine transporter but are not required for its protein kinase C dependent endocytosis. Traffic. 2013; 14:709–24. [PubMed: 23418867]
38. Gabriel LR, et al. Dopamine transporter endocytic trafficking in striatal dopaminergic neurons: differential dependence on dynamin and the actin cytoskeleton. J Neurosci. 2013; 33:17836–46. [PubMed: 24198373]
39. Mazei-Robison MS, et al. Anomalous dopamine release associated with a human dopamine transporter coding variant. J Neurosci. 2008; 28:7040–6. [PubMed: 18614672]
40. Das R, Baker D. Macromolecular modeling with rosetta. Annu Rev Biochem. 2008; 77:363–82. [PubMed: 18410248]
41. Gracia, L. RMSDTT: RMSD Trajectory Tool. 2.5 ed. Weill Medical College of Cornell University, Department of Physiology and Biophysics; 2005.
42. Humphrey W, Dalke A, Schulten K. VMD: visual molecular dynamics. J Mol Graph. 1996; 14:33–8. 27–8. [PubMed: 8744570]
43. Earl DJ, Deem MW. Parallel tempering: theory, applications, and new perspectives. Phys Chem Chem Phys. 2005; 7:3910–6. [PubMed: 19810318]

44. Kiessling V, Wan C, Tamm LK. Domain coupling in asymmetric lipid bilayers. Biochim Biophys Acta. 2009; 1788:64–71. [PubMed: 18848518]
45. Sali A, Blundell TL. Comparative protein modelling by satisfaction of spatial restraints. J Mol Biol. 1993; 234:779–815. [PubMed: 8254673]
46. Sharp KA, Honig B. Electrostatic interactions in macromolecules: theory and applications. Annu Rev Biophys Biophys Chem. 1990; 19:301–32. [PubMed: 2194479]
47. Chaikin, PM.; Lubensky, TC. Principles of Condensed Matter Physics. Cambridge university press; Cambridge: 2000.
48. Mackerell AD Jr. Feig M, Brooks CL 3rd. Extending the treatment of backbone energetics in protein force fields: limitations of gas-phase quantum mechanics in reproducing protein conformational distributions in molecular dynamics simulations. J Comput Chem. 2004; 25:1400–15. [PubMed: 15185334]
49. Friggi-Grelin F, et al. Targeted gene expression in Drosophila dopaminergic cells using regulatory sequences from tyrosine hydroxylase. J Neurobiol. 2003; 54:618–27. [PubMed: 12555273]
50. Wang JW, Beck ES, McCabe BD. A modular toolset for recombination transgenesis and neurogenetic analysis of Drosophila. PLoS One. 2012; 7:e42102. [PubMed: 22848718]

Europe PMC Funders Author Manuscripts

Europe PMC Funders Author Manuscripts

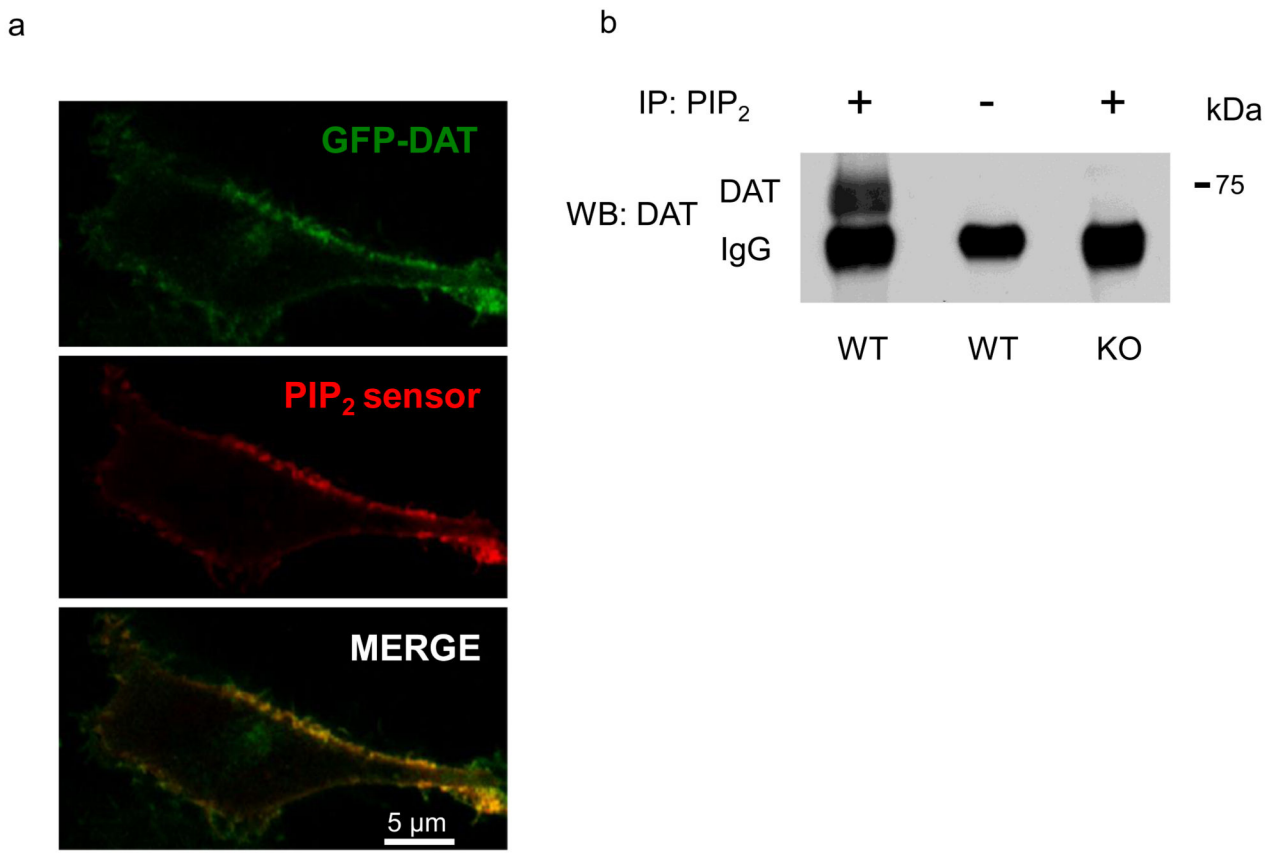

Figure 1. PIP_2 interacts with hDAT

(a) hDAT and PIP_2 co-localize at the plasma membrane. In hDAT expressing cells, GFP-hDAT (green) co-localizes (yellow) at the plasma membrane with the PIP_2 sensor $PHPLC_{\delta}$-mRFP (red) (representative image from three live experiments with of 10-15 cells imaged per experiment). **(b)** PIP_2 associates with endogenous mouse DAT in striatal tissue. In striatal lysate, DAT was detected in PIP_2 immunoprecipitates using an anti-DAT antibody (+). DAT immunoreactivity was absent in the beads fraction (−) and in PIP_2 immunoprecipitates from DAT knock out (KO) animals (endogenous mouse IgG is observed) (representative of n = 3). Full blot is in Supplementary Figure 7.

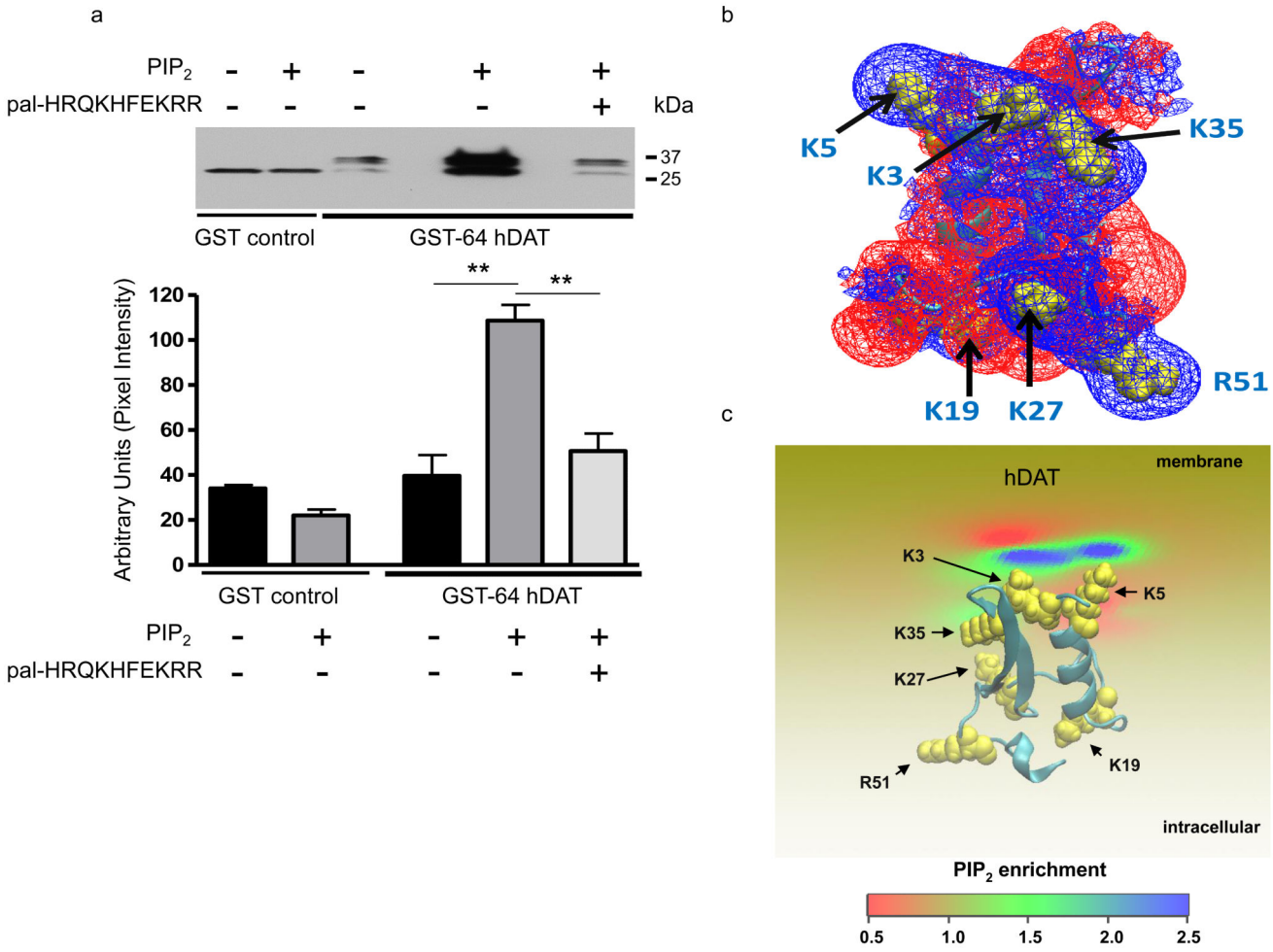

Figure 2. hDAT-PIP_2 electrostatic interactions are mediated by the hDAT N-terminus

(a) hDAT N-terminus binds directly to PIP_2. GST-64 hDAT is enriched in liposome-pull downs with liposomes containing PIP_2 (+) as compared to liposomes lacking PIP_2 (−) (** = $p \leq 0.01$ by one-way ANOVA followed by Bonferroni post-hoc test; n = 3; mean ± s.e.m.). Pull down of GST control was not altered by the presence (+) of absence (−) of PIP_2 in the liposomes ($p \geq 0.05$ by one-way ANOVA followed by Bonferroni post-hoc test; n = 3; mean ± s.e.m.). Preincubation of liposome containing PIP_2 with 3 μM of pal-HRQKHFEKRR (+) inhibited the pull down of GST-64 hDAT with liposomes containing PIP_2 (** = $p \leq 0.01$ by one-way ANOVA followed by Bonferroni post-hoc test; n = 3). Full blot is in Supplementary Figure 8. **(b)** Electrostatic potential (EP) isosurfaces (+1kT/e (+ charge)) shown as *blue wireframes* and (−1kT/e (− charge)) as *red wireframes* calculated for the predicted structure of the wild type N-terminus. **(c)** View from the intracellular side of the N-terminus (model) adsorbing on the lipid membrane. For clarity, the orientation of the N-terminus in panel (c) was obtained by a 180° rotation of the N-terminus configuration shown in panel (b). The level of the PIP_2 segregation by the N-terminus is expressed as the ratio of local and ambient lipid fraction values, and illustrated in color code (cold colors represent an enrichment of PIP_2). The positive residues in the N-terminus (yellow) that attract PIP_2 electrostatically are highlighted.

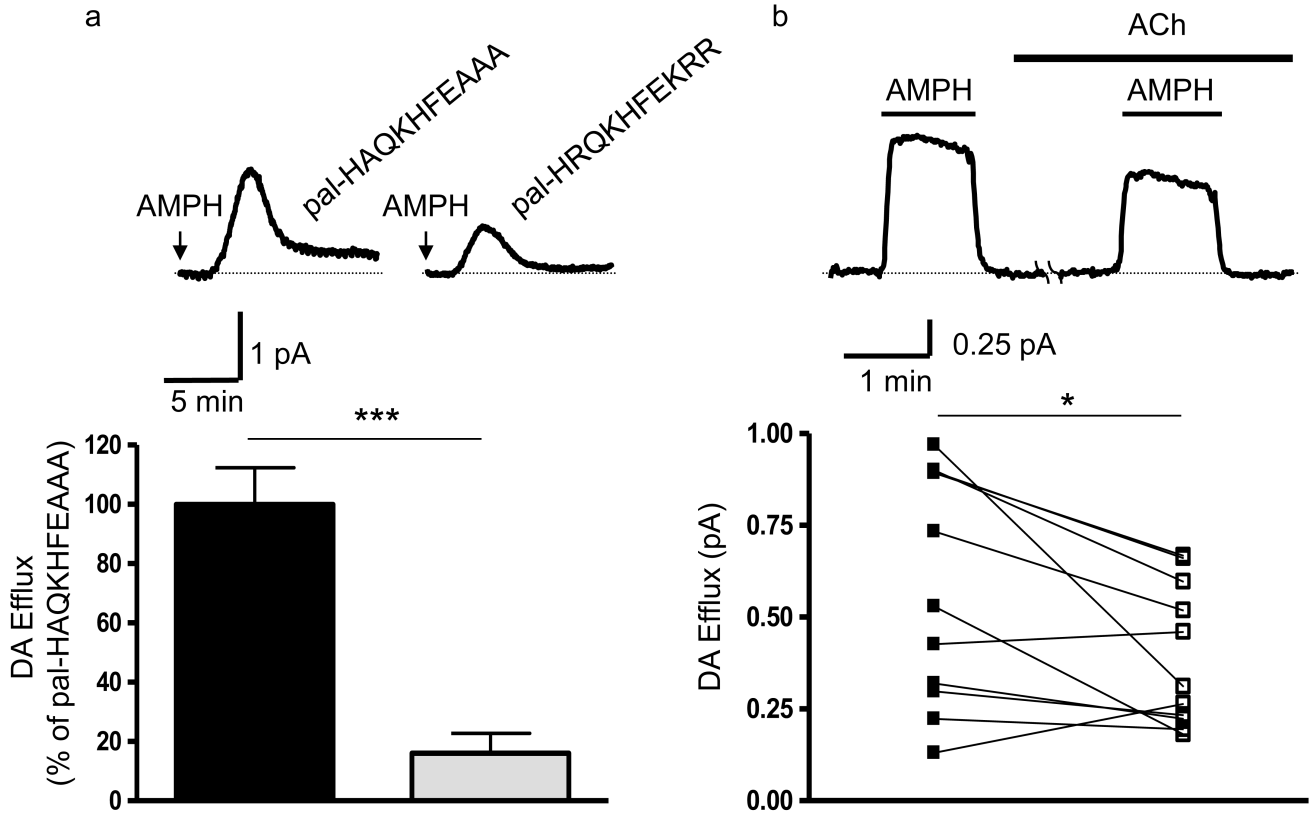

Figure 3. Sequestration or depletion of PIP_2 inhibits AMPH-induced DA efflux

(a) Sequestering PIP_2 with pal-HRQKHFEKRR decreases AMPH-induced DA efflux. Top: representative traces from stably transfected hDAT cells after patch delivery of 3 μM control peptide (pal-HAQKHFEAAA) or PIP_2 sequestering peptide (pal-HRQKHFEKRR) to the cytoplasm of the cell. Arrows indicate the application of 10 μM AMPH. Bottom: quantitation of amperometric peak currents for the two different treatments. Data are expressed as percentage of vehicle control (*** = $p \leq 0.0001$ by Student's t-test; n = 7; mean ± s.e.m.). **(b)** Depleting PIP_2 levels reduces AMPH-induced DA efflux. Top: representative trace of responses to 1 μM AMPH in stably transfected hDAT cells, co-expressing the human muscarinic acetylcholine receptor 1 (hM1R), before and after exposure to 100 μM acetylcholine (ACh). Bottom: quantitation of the amperometric peak currents representing AMPH-induced DA efflux before and after ACh-dependent PIP_2 depletion (* = $p \leq 0.05$ by Student's t-test; n = 11).

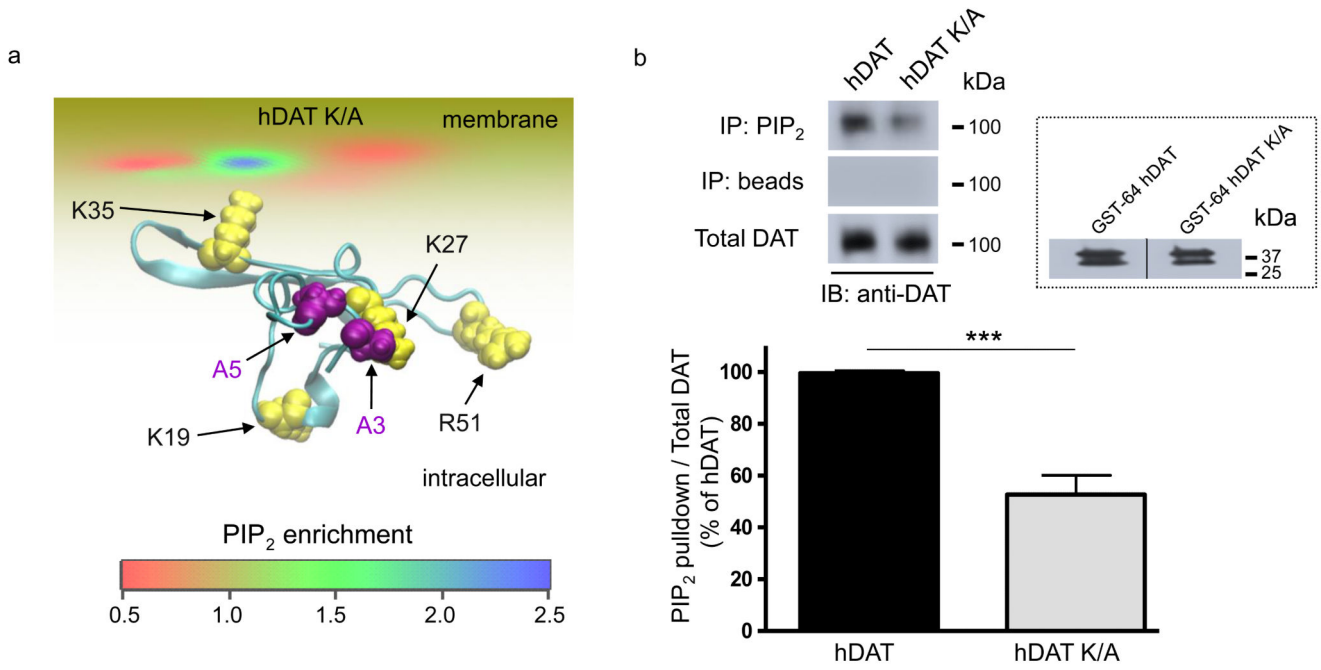

Figure 4. hDAT N-terminal Lys regulate hDAT-PIP_2 interaction

(a) Mutating hDAT N-terminal residues Lys3 and Lys5 to uncharged Ala (hDAT K/A) disrupts PIP_2 segregation to the N-terminus. View from the intracellular side of the N-terminus of hDAT K/A adsorbing on the lipid membrane. The level of PIP_2 segregation by the N-terminus residues is expressed as the ratio of local and ambient lipid fraction values and illustrated in color code, with cold colors representing an enrichment of PIP_2. **(b)** N-terminal Lys residues mediate hDAT-PIP_2 interaction. Top: PIP_2 immunoprecipitates from hDAT and hDAT K/A cells were immunoblotted for DAT (top lane). The beads fraction supports absence of non-specific binding (middle lane). Bottom lane shows total DAT proteins. Full blot is in Supplementary Figure 9. Bottom: quantitation of PIP_2 pulldown band intensities normalized to the respective total DAT and expressed as a percentage hDAT (*** = $p \leq 0.001$ by Student's t-test; n = 4; mean ± s.e.m.). *Inset:* Representative blot for GST-64 hDAT and GST-64 hDAT K/A in pull downs with liposomes containing PIP_2. Full blot is in Supplementary Figure 9.

Europe PMC Funders Author Manuscripts

a

	hDAT	hDAT K/A
V_{max} (pmol/min/10^5 cells)	6.85 ± 0.75	6.94 ± 0.62
K_m (μM)	2.18 ± 0.22	2.05 ± 0.09

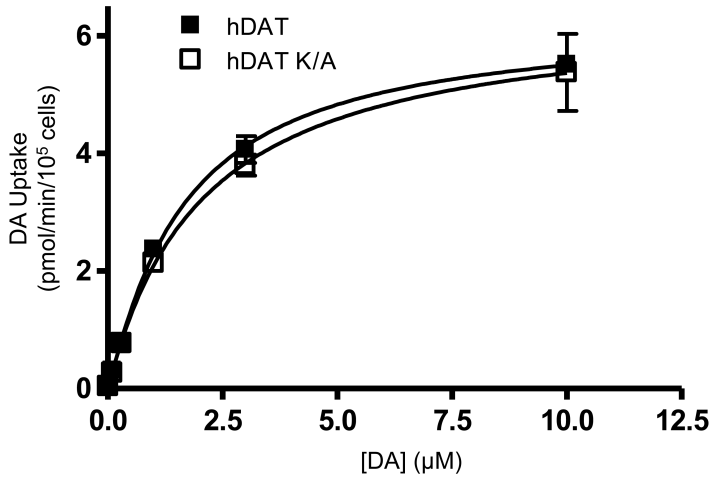

b

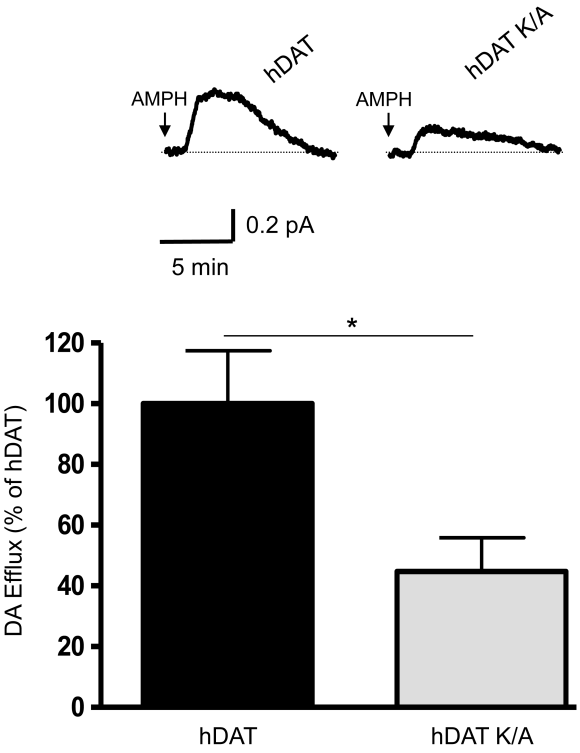

Figure 5. N-terminal Lys3 and Lys5 regulate specific modalities of hDAT function

(a) hDAT K/A exhibits normal DA uptake function. Top: kinetic parameters (V_{max} and K_m) for hDAT and hDAT K/A (V_{max}: $p \geq 0.92$ by Student's t-test; n = 3, in triplicate; K_m: $p \geq 0.62$ by Student's t-test; n = 3, in triplicate; mean ± s.e.m.). Bottom: representative plot of [^{3}H]DA uptake kinetics in hDAT (filled squares) and hDAT K/A (empty squares) cells ($p \geq 0.05$, by two-way ANOVA followed by Bonferroni post-test; in triplicate; mean ± s.e.m.). **(b)** hDAT K/A has reduced AMPH-induced DA efflux. Top: representative AMPH-induced amperometric currents recorded from hDAT and hDAT K/A cells. Arrows indicate application of 10 μM AMPH. Bottom: quantitation of AMPH-induced DA efflux. Data are represented as maximal DA efflux expressed as percent of the DA efflux recorded in hDAT controls (* = $p \leq 0.05$ by Student's t-test; n = 7-8; mean ± s.e.m.).

Europe PMC Funders Author Manuscripts

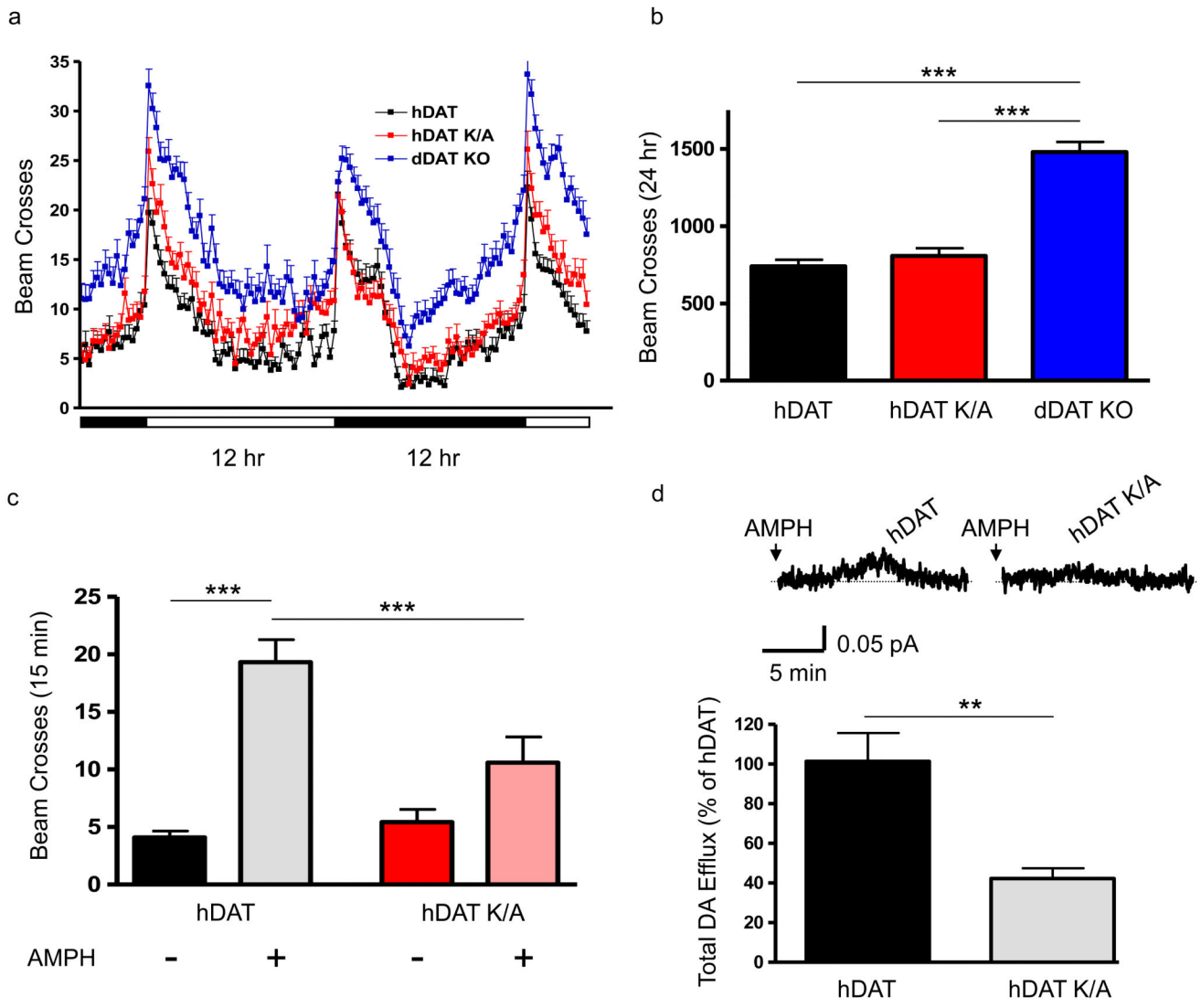

Figure 6. Expression of hDAT K/A in *Drosophila* dopaminergic neurons does not affect circadian locomotor activity yet impairs AMPH-induced locomotion and neuronal DA efflux

hDAT or hDAT K/A was expressed in DA neurons of dDAT KO flies. **(a)** Locomotion was assayed over 32 hours during the light (horizontal white bars) or dark (horizontal black bars) cycle. Flies expressing dDAT KO (blue squares) were hyperactive with respect to flies expressing wild type hDAT (black squares) and flies expressing hDAT K/A (red squares) (beam breaks binned in 15 minute intervals; n = 31-42; mean ± s.e.m.). **(b)** Quantitation of total beam crosses over 24 hours for hDAT, hDAT K/A, and dDAT KO flies (*** = $p \leq 0.001$ by one-way ANOVA followed by Bonferroni post-test; n = 31-42; mean ± s.e.m.). **(c)** AMPH did not cause a significant increase in locomotion in hDAT K/A flies compared to vehicle control ($p \geq 0.05$ by one-way ANOVA followed by Bonferroni post-test; n = 25-49; mean ± s.e.m.). In hDAT flies, AMPH induced a significant increase in locomotion compared to vehicle control (*** = $p \leq 0.001$ by one-way ANOVA followed by Bonferroni post-test; n= 25-60; mean ± s.e.m.). **(d)** hDAT K/A *Drosophila* DA neurons show reduced AMPH-induced DA efflux. Dopaminergic neurons were selected by fluorescence

microscopy since the expression of mCherry was driven by TH-GAL4. Top: representative amperometric currents from hDAT and hDAT K/A neurons. Arrows indicate application of 1 μM AMPH. Bottom: quantitation of total AMPH-induced DA efflux. Data represented as cumulative DA efflux expressed as percent of DA efflux from hDAT neurons (** = $p \leq 0.01$ by Student's t-test; n = 4-5; mean ± s.e.m.).

Europe PMC Funders Author Manuscripts